Materials Science in Additive Manufacturing

ORIGINAL RESEARCH ARTICLE

Inconel 718-CoCrMo bimetallic structures through directed energy deposition-based additive manufacturing

Cory Groden[1], Victor Champagne[2], Susmita Bose[1], Amit Bandyopadhyay[1]*

[1]W. M. Keck Biomedical Materials Research Laboratory, School of Mechanical and Materials Engineering, Washington State University Pullman, WA 99164, USA

[2]US Army Research Laboratory, Weapons and Materials Research Directorate, Aberdeen Proving Ground, MD, USA

Abstract

Bimetallic structures and coatings through additive manufacturing (AM) have demonstrated a high degree of freedom for tailoring properties depending on the application. In this study, Inconel 718 and CoCrMo were used as both are common alloys and exhibit unique properties, such as high-temperature oxidation, wear, and fatigue resistance. Using directed energy deposition-based metal AM, bimetallic structures containing these two alloys were manufactured, and the resulting structures exhibited no intermetallic phase formation, cracking, or porosity. Scanning electron microscopy and energy dispersive spectroscopy revealed a smooth elemental transition between the two compositions. Hardness testing showed a linear transition in the interfacial zone, validating no brittle intermetallic phase formation. Compression testing and fracture surface analysis revealed that the failures were not dependent on the interface properties. High-temperature oxidation showed no distinct effect on the interface, a firmly attached chromium oxide layer on the Inconel 718 side and a loosely attached chromium oxide layer on the CoCrMo side. There was also evidence of pit formation on the Inconel 718 surface, but not on the CoCrMo. These findings confirm a stable bimetallic system in which one of the two alloys can be used on the other material to improve the structure's high-temperature oxidation or wear/corrosion resistance.

Keywords: Additive manufacturing; Three-dimensional printing; Directed energy deposition; Cobalt-chromium molybdenum alloy; Inconel 718; Bimetallic structures

***Corresponding author:**
Amit Bandyopadhyay
(amitband@wsu.edu)

Citation: Groden C, Champagne V, Bose S, *et al.,* 2022, Inconel 718-CoCrMo bimetallic structures through directed energy deposition-based additive manufacturing. *Mater Sci Add Manuf*, 1(3):18. https://doi.org/10.18063/msam.v1i3.18

Received: September 1, 2022

Accepted: September 14, 2022

Published Online: September 27, 2022

1. Introduction

Advances in metal additive manufacturing (AM) technology have allowed designing multi-material structures to impart unique and site-specific properties for various applications. For example, AM-processed FeCrAl coating on a Zr alloy increased the oxidation resistance by a factor of 50[1]. It has been reported that a 30Cr15MoY alloy steel on a C45 substrate increased the corrosion resistance of neat C45 steel[2]. For strength and thermal conductivity, adding a tungsten alloy coating to Inconel 718 increased the strength and thermal conductivity compared to pure Inconel 718[3]. A GRCop84 coating on Inconel 718 increased thermal conductivity by 300% more than pure Inconel 718[4].

Finally, for increased bioactivity, AM-processed titanium (Ti)-tantalum (Ta) bimetallic structure has shown a significant improvement in biocompatibility similar to pure Ta[5]. A recent review documents many such performance enhancements through AM-processed bimetallic and multi-material structures that highlight the innovation opportunities using AM with the next-generation metallic materials[6]. The interface between the coating and the bulk material can form various intermetallic compounds, which have been shown to increase the strength of some bimetallic systems, such as Ti6Al4V/Al12Si and Ti/Ni[7,8]. However, this interfacial behavior can be detrimental in some cases, which has prompted studies to understand better and model the behavior of these bimetallic systems[9]. In addition, research has been conducted to manufacture multi-material and bimetallic systems more efficiently to be better suited for industry[10].

Inconel 718 is a nickel-based superalloy consisting of about 55% nickel (Ni), 18% chromium (Cr), 18% iron (Fe), 5% niobium (Nb), and 3% molybdenum (Mo). This alloy is used extensively in aerospace applications due to its excellent high-temperature strength, along with corrosion and oxidation resistance[11]. Inconel 718 is a standard alloy used in AM due to its excellent weldability[12]. This alloy is particularly strong for the formation of the γ' (Ni_3Ti and Ni_3Al), the γ" (cubic Ni_3Nb), and the δ (orthorhombic Ni_3Nb) phases, all of which have been observed in heat-treated Inconel 718 samples that were printed by selective laser melting (SLM)[13]. Different heat treatments can control the amount of these phases formed in Inconel 718[14-16]. This allows manufacturers to tailor the properties of Inconel 718 depending on the application and further demonstrates the versatility of this alloy. The corrosion resistance of Inconel 718 comes from the Cr and Mo, which forms a surface passivation layer limiting oxygen flow into the bulk structure. Because of microstructural and phase evolutions, corrosion resistance for Inconel 718 also depends on the manufacturing and post-processing methods used. It has been reported that excessive carbide formation during solution treatment caused Cr and Mo depletion throughout the bulk Inconel 718[17]. Oxidation resistance is typically attributed to the Cr_2O_3 film, which prevents oxygen diffusion into the bulk structure; however, a NbO film also forms at temperatures higher than 800°C to further aid oxidation resistance[18].

Cobalt-chromium molybdenum (CoCrMo) alloy consists of around 60% cobalt, 30% Cr, and 5% Mo, with 5% being other elements such as Ti. Due to its excellent wear and corrosion resistance, this alloy is used in cutting tools and other applications requiring better wear resistance, such as articulating surfaces of biomedical implants and dental crowns[19-21]. However, this alloy's high hardness and wear resistance make it very difficult to machine[22]. As a result, many studies look at the cutting force and anisotropic effects to explain how to properly machine these alloys without compromising the alloy surface or the milling tools[23,24]. The strengthening mechanism in CoCrMo alloy comes from the various carbides, such as $Co_{23}C_6$ and Cr_6C[25]. Therefore, the properties of CoCrMo alloys can be altered using different heat treatments, which results in various carbide formations[26,27]. The oxidation resistance of CoCrMo at high temperatures is not well reported; however, the alloy's carbide forming abilities and the chromium oxide layer offer good oxidation resistance.

Since CoCrMo is wear- and corrosion-resistant and Inconel 718 is high-temperature oxidation-resistant, a coating of one of these materials may prove effective in increasing the bulk and surface properties of the bimetallic structures. In cases where a strong bulk structure is needed with high oxidation resistance, Inconel 718 coating on CoCrMo would be preferred. A CoCrMo coating on Inconel 718 could be preferred in cases where superior corrosion resistance is needed. A recent study using laser powder bed fusion (L-PBF) of Inconel 718 and CoCrMo functionally graded structure exhibited low porosity and smooth composition transitions[28]; however, there is still a knowledge gap on processing-structure-properties relationships of DED-manufactured bimetallic structures of Inconel 718 and CoCrMo. Addressing this gap is the primary focus of this research. Inconel 718 and CoCrMo bimetallic structures were manufactured by DED-based AM and were subjected to various tests for microstructure and phase analysis, hardness, compression testing, and measuring high-temperature oxidation resistance. Figure 1 outlines the processing strategies for the Inconel 718 and CoCrMo bimetallic structures using DED.

2. Materials and methods

2.1. Directed energy deposition (DED) of bimetallic structures

Inconel 718 and CoCrMo bimetallic structures were manufactured using a powder-based DED printer (FormAlloy, CA). The computer uses a G-code input file derived from a computer-aided design (CAD) file containing the shape information. This G-code input file dictates the machine parameters while printing, including speed, layer thickness, laser power, powder flow rate, and shield gas flow rate, which prevents powders from melting onto the nozzle and clogging it. These alloys were printed onto 316L stainless steel substrate. Inconel 718 powder (Powder Alloy Corporation, Ohio) was used with a particle size of 50–150 μm. CoCrMo

powder (Stellite Coatings, Goshen, IN) was used with a particle size range of 50–100 μm. The bimetallic structures were optimized until the part height was close to the theoretical height. The final parameters for each sample are listed in Table 1.

2.2. Characterization of bimetallic samples

Bimetallic samples were cut in half and underwent a typical grinding or polishing procedure. The samples were then imaged using a field emission scanning electron microscope (FESEM, FEI-SIRION, Portland, OR) to determine if any defects existed at the interface. Using the energy dispersive spectroscopy (EDS; EDAX), elemental maps were obtained to examine elemental distributions at the interface. Vicker's hardness testing (Penn Tool Co, NJ) was performed along the interface and compared to the base materials' hardness. At least 15 measurements were taken for each point. For the compression tests, an Instron servohydraulic compression tester was used to determine the stress-strain curves for the longitudinal and transverse bimetallic samples and the base materials using a strain rate of 1.3 mm/min. For the oxidation tests, a muffle furnace with no other additions was used to oxidize samples for 96 h at 800°C and then underwent the same characterization process mentioned above.

3. Results

3.1. Microstructural variations

Figure 2 shows a stereoscope image of the bimetallic sample on a 316L substrate and the SEM/EDS analysis of the interface. A small but distinct interface is formed between the CoCrMo and substrate. The same can be observed between the Inconel 718 and CoCrMo junction,

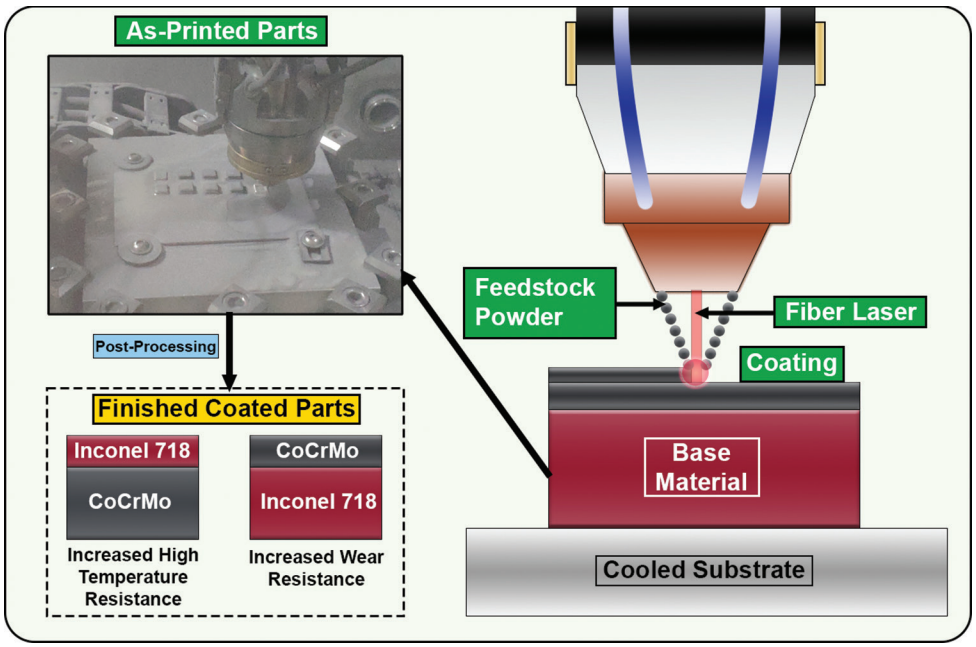

Figure 1. Processing strategies of bimetallic structures of Inconel 718-CoCrMo using laser directed energy deposition process.

Table 1. Final DED build parameters for Inconel 718, CoCrMo, and bimetallic samples

Type of sample	Inconel 718 scanning speed (mm/min)	CoCrMo scanning speed (mm/min)	Inconel 718 laser power (W)	CoCrMo laser power (W)	Inconel 718 flow rate (mm/s)	CoCrMo flow rate (m m/s)	Layer height (mm)
Oxidation and Characterization Bimetallic	1200	1600	350	350	0.5	0.6	0.1
Inconel 718 Compression	1600		350		0.5		0.1
CoCrMo Compression		600		300		0.5	0.25
Transverse Bimetallic	600	1200	300	300	0.25	0.5	0.25
Longitudinal Bimetallic	800	1200	300	300	0.3	0.5	0.2

DED: Directed energy deposition

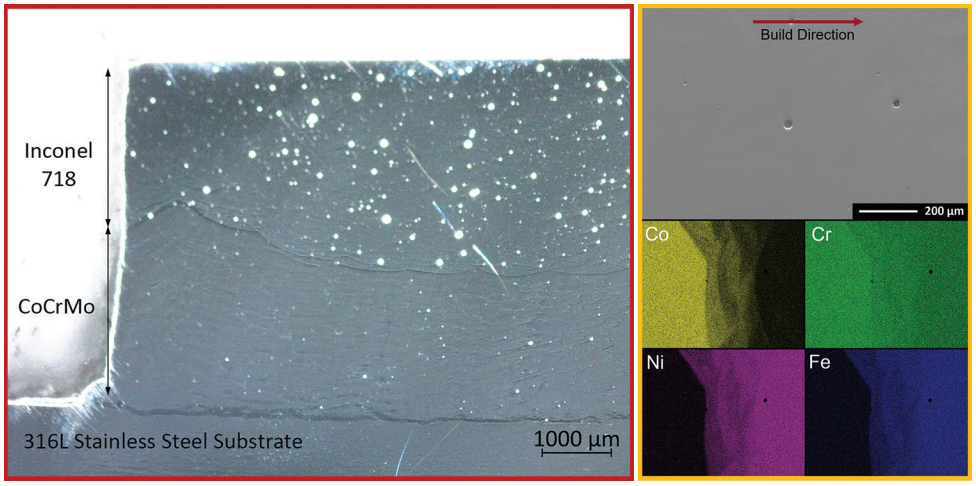

Figure 2. (Left) Inconel 718 – CoCrMo bimetallic structure. (Right) SEM/EDS analysis of the bimetallic interface. Note that the interface is not visible in the SEM micrograph, but the compositional variations mark the interface in the EDS mapping.

with the bimetallic interface appearing smaller than the substrate interface. The illuminated circles are tiny gas pores, which are more frequent and extensive in the Inconel 718 region than in the CoCrMo region. For the SEM image, a seemingly blank photo is observed with no qualitative distinction between the two materials and the interface. However, the EDS mapping indicates a relatively smooth transition between the elements, meaning there is little to no elemental segregation. No cracking or other defects are observed at the interface, which confirms that these materials are compatible[28].

3.2. Hardness

Vicker's hardness tests were conducted on polished samples and the results are shown in Figure 3. The tests show that the base hardnesses in the Inconel 718 and CoCrMo zones were about 260 HV and 430 HV, respectively. A hardness profile was established, measuring at every 50 µm distance within the interface zone until the pure alloys were reached. The profile shows a linear variation within the interface region. The linear profile confirms no brittle intermetallic phase formations and reveals that the interface is about 150 µm wide.

3.3. Compression testing

Figure 4 shows stress-strain curves for the four types of non-heat treated compression samples. The test's primary purpose was to understand the role of the interface in compressive deformation behavior. It was found that the interface properties did not limit the compressive deformation in bimetallic structures but were instead controlled by the bulk materials. The transverse bimetallic samples had the worst yield strength, with the base CoCrMo sample performing the best. The Inconel 718 samples did not fail, so the plot only displays up to 0.4 strain for that sample. The failure behavior of the two bimetallic structures is illustrated in Figure 5.

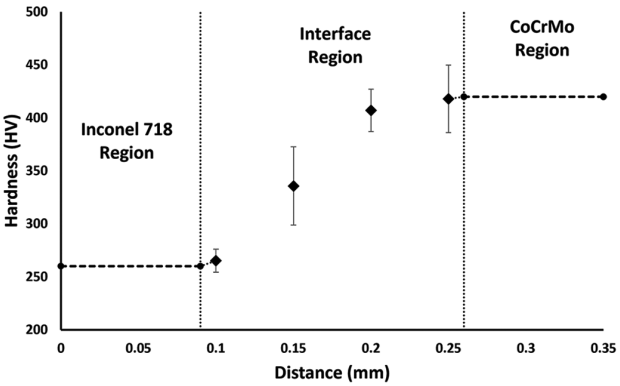

Figure 3. Vicker's hardness profile of Inconel 718-CoCrMo bimetallic structure.

3.4. Oxidation studies of bimetallic samples

For the oxidation and followed by hardness measurements, samples were tested at 800°C for 96 h. No significant variations in hardness were observed. Only a slight decrease in hardness (430 HV to 400 HV) was observed in the CoCrMo part, which occurred as a byproduct of the oxidation test since recrystallization would also occur. Figure 6 shows the SEM/EDS analysis of the oxide layer formed in each constituent. For Inconel 718, a strongly adherent chromium oxide layer was formed along with some pits. This pitting resulted from the depletion of Cr near the interface, which made the material under the oxide layer prone to the effects of oxidation. For the CoCrMo side, spalling was observed, meaning that the oxide layer was not strongly attached to the base material. Furthermore, a Cr depletion zone was not observed in the CoCrMo part.

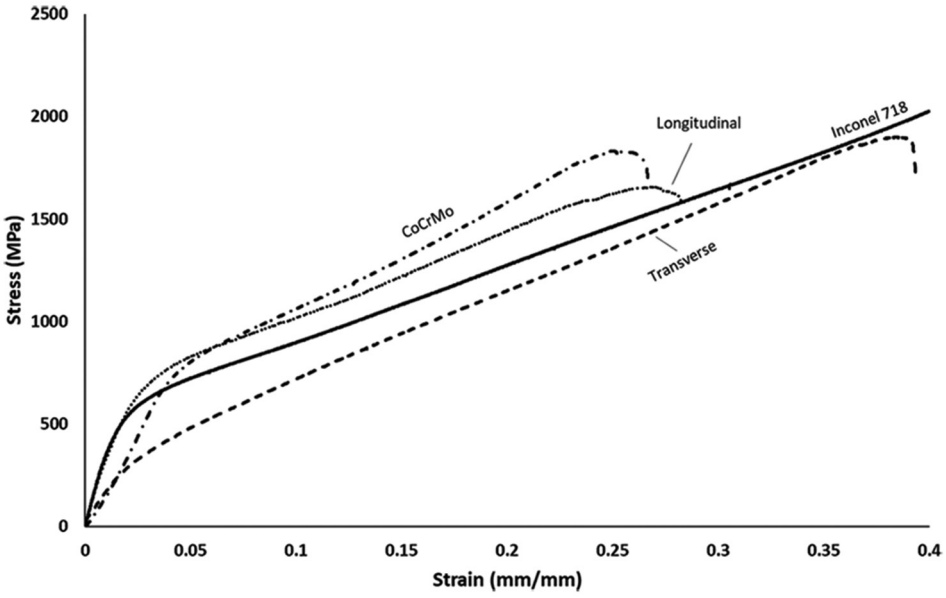

Sample	Inconel 718	CoCrMo	Transverse bimetallic	Longitudinal bimetallic
Yield strength	498±34	600±103	408±75	533±65

Figure 4. Stress-strain curves for each compression sample type. Note that only one of each sample type is shown and that the Inconel 718 base sample did not fail and therefore is only plotted until 0.4 strain.

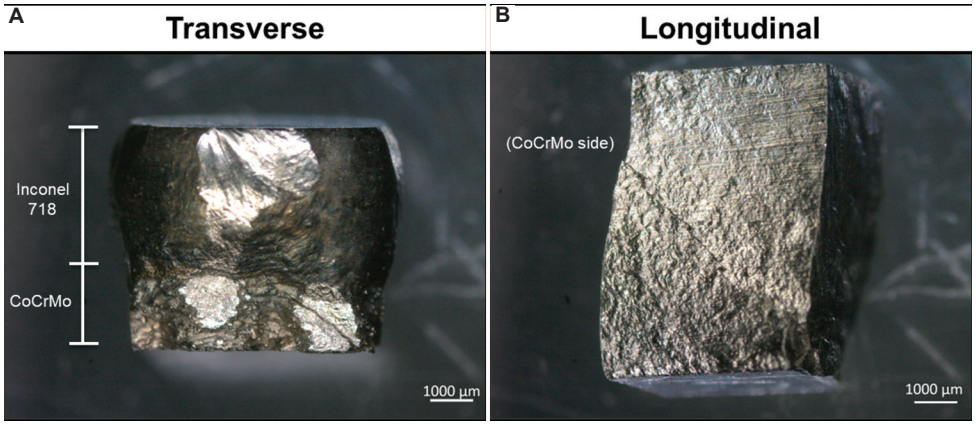

Figure 5. (A) Failure behavior of the transverse bimetallic sample. Cracking is observed in the CoCrMo part at the bottom right. **(B)** Failure behavior of the longitudinal bimetallic sample, in which there is cracking on the CoCrMo side at a 45° angle.

4. Discussion

The laser DED process is used to form bimetallic structures of Inconel 718 to CoCrMo. The results show that the Inconel 718 and CoCrMo form a stable interface. This indicates that using a coating of one or the other could tailor a structure with specific properties depending on the need, with the CoCrMo coating working better for wear and corrosion resistance applications with static conditions and with the Inconel 718 coating working better for high-temperature oxidation resistance applications with dynamic conditions. Furthermore, the microstructural findings of this study are in line with published data where functionally graded structures were printed through powder bed fusion (PBF)[28].

It is essential to discuss what coating should be used for what application. Inconel 718 coating on CoCrMo would work better in environments with dynamic conditions in high-temperature environments. This is due to the oxide layer in Inconel 718 being firmly attached, unlike

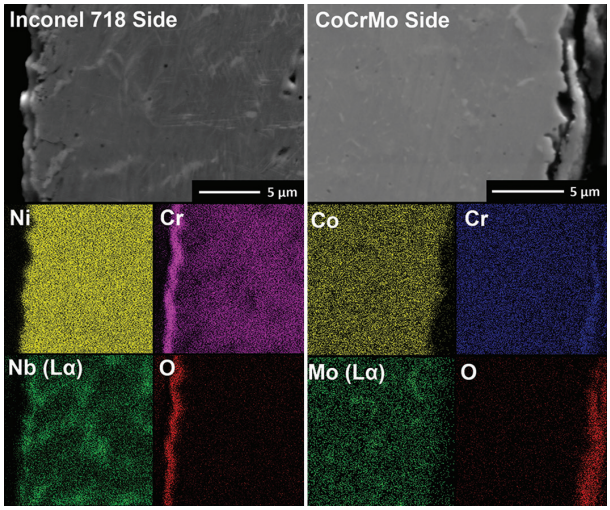

Figure 6. SEM and EDS images of the oxidation of the Inconel 718 and CoCrMo bimetallic sample. The Inconel 718 oxide layer is on the left of the micrograph, where a strongly adherent oxide layer is seen. The CoCrMo oxide layer is on the right, where spalling of the oxide layer can be seen.

the CoCrMo oxide layer. Although it was found that the CoCrMo showed less oxidation damage compared to Inconel 718, the Inconel 718 coating oxide layer would be able to resist further oxidation damage, but the coating would also be able to keep the CoCrMo oxide layer from being washed away, preventing degradation of the bulk structure. In the opposite scenario with a CoCrMo coating on Inconel 718, this structure would be best suited for corrosive environments and situations with high wear, as the corrosion and wear resistance of CoCrMo are unmatched compared to most alloys.

Wen *et al.* recently published functionally graded structures of Inconel 718 and CoCrMo printed using laser PBF[28]. In this study, we produced defect-free and low-porosity structures without any concerns related to the compatibility of the base materials. Our results also show a compatible interface between Inconel 718 and CoCrMo, even with the case of direct bimetallic transition, which is much more prone to issues arising from material incompatibility due to a sharp change in composition. The hardness of the CoCrMo part in our study compared to the FGM study differed by about 30 HV (420 HV compared to 400 HV, respectively), while the same for Inconel 718 part differed by 90 HV (360 HV compared to 270 HV). However, this difference is expected as the printing techniques are different and it is evident that different amounts of carbides formed in the FGM parts compared to the bimetallic parts due to faster cooling rates in DED. Finally, the stress-strain plots in each study showed considerable failure strain, reinforcing the notion that unwanted intermetallic phases are not a concern for these bimetallic structures.

Although oxidation kinetics are well understood for single material systems, more studies are needed to understand the oxidation resistance of coated or bimetallic systems. For single materials, the oxidation resistance can significantly vary depending on factors, such as oxide formation rate, defects, and mean free path of oxygen.[29]. The oxide layer's composition also matters significantly due to the defect density in the said oxide layer. For example, chromium oxide layers typically exhibit a very low defect density, preventing oxygen diffusion[30-32]. Material constants are typically determined experimentally by fitting a curve to the data. In the case of parabolic-type oxidation, the rate equation is given by:

$$\frac{dx}{dt} = \frac{Kp}{x}$$

Where Kp is the rate constant, and x is the scale thickness[29]. Most metallic alloys follow this parabolic behavior due to the continual formation of the oxide layer, while ceramic materials follow a more linear relationship. In the case of an alloy's thin coating, oxygen's mean free path will be significantly higher to diffuse to the bulk material under the coating. However, the constants could potentially be determined by first determining the oxidation constants for the coating, then using it as a correction curve for the coated structure. In this work, Inconel 718 coating on CoCrMo proved to be a better combination to enhance oxidation resistance of the bimetallic structure due to the strongly adherent oxide layer on Inconel 718 even after 96 h at 800°C.

5. Conclusions

Inconel 718-CoCrMo was successfully manufactured using the laser DED-based AM. No difficulty was observed in printing these structures, even during optimization, and the finished parts had low porosity without any cracking. The interface could not be distinguished using SEM imaging but was revealed in EDS mapping of elemental transitions. Hardness testing revealed a smooth yet brief transition between the two alloys. Compression testing showed that the CoCrMo had the highest yield strength of the four structures tested and determined that the compression behavior was not dependent on the bimetallic interface. Oxidation tests showed that the bimetallic interface was not affected by the high temperatures and revealed that the Inconel 718 formed a firmly attached chromium oxide layer, while the CoCrMo showed spalling of the same oxide layer.

Acknowledgments

The authors thank JCDREAM (Seattle, WA) for a capital equipment grant to purchase the directed energy deposition (DED)-based metal 3D Printer at WSU.

Funding

The authors want to acknowledge financial support from the Army Research Laboratory under grant number W911NF2020206. The views and conclusions contained in this document are those of the authors and should not be interpreted as representing the official policies, either expressed or implied, of the Army Research Laboratory or the U.S. Government. The U.S. Government is authorized to reproduce and distribute reprints for Government purposes, notwithstanding any copyright notation herein.

Conflict of interest

The authors declare no conflicts of interest.

Author contributions

Conceptualization: Victor Champagne, Amit Bandyopadhyay
Data curation: Cory Groden
Funding acquisition: Susmita Bose, Amit Bandyopadhyay
Investigation: Cory Groden
Supervision: Susmita Bose, Amit Bandyopadhyay
Writing – original draft: Cory Groden
Writing – review & editing: Victor Champagne, Susmita Bose, Amit Bandyopadhyay

References

1. Kim IH, Jung YI, Kim HG, *et al*., 2021, Oxidation-resistant coating of FeCrAl on Zr-alloy tubes using 3D printing direct energy deposition. *Surf Coat Technol*, 411: 126915.

   https://doi.org/10.1016/j.surfcoat.2021.126915

2. Shang F, Chen S, Zhou L, *et al*., 2021, Effect of laser energy volume density on wear resistance and corrosion resistance of 30Cr15MoY alloy steel coating prepared by laser direct metal deposition. *Surf Coat Technol*, 421: 127382.

   https://doi.org/10.1016/j.surfcoat.2021.127382

3. Groden C, Traxel KD, Afrouzian A, *et al*., 2022, Inconel 718-W7Ni3Fe bimetallic structures using directed energy deposition-based additive manufacturing. *Virtual Phys Prototyp* 17: 170–180.

   https://doi.org/10.1080/17452759.2022.2025673

4. Onuike B, Heer B, Bandyopadhyay A, 2018, Additive manufacturing of inconel 718-copper alloy bimetallic structure using laser engineered net shaping (LENS™). *Addit Manuf*, 21: 133–140.

   https://doi.org/10.1016/j.addma.2018.02.007

5. Traxel KD, Bandyopadhyay A, 2021, Modeling and experimental validation of additively manufactured tantalum-titanium bimetallic interfaces. *Mater Des*, 207: 109793.

   https://doi.org/10.1016/j.matdes.2021.109793

6. Bandyopadhyay A, Zhang Y, Onuike B, 2022, Additive manufacturing of bimetallic structures. *Virtual Phys Prototyp*, 17: 256–294.

   https://doi.org/10.1080/17452759.2022.2040738

7. Zhang Y, Bandyopadhyay A, 2019, Direct fabrication of bimetallic Ti6Al4V+Al12Si structures via additive manufacturing. *Addit Manuf*, 29: 100783.

   https://doi.org/10.1016/j.addma.2019.100783

8. Afrouzian A, Groden CJ, Field DP, *et al*., 2022, Additive manufacturing of Ti-Ni bimetallic structures. *Mater Des*, 215: 110461.

   https://doi.org/10.1016/j.matdes.2022.110461

9. Yao L, Huang S, Ramamurty U, *et al*., 2021, On the formation of "Fish-Scale" morphology with curved grain interfacial microstructures during selective laser melting of dissimilar alloys. *Acta Mater*, 220: 117331.

   https://doi.org/10.1016/j.actamat.2021.117331

10. Sing SL, Huang S, Goh GD, *et al*., 2021, Emerging metallic systems for additive manufacturing: *In-situ* alloying and multi-metal processing in laser powder bed fusion. *Prog Mater Sci*, 119: 100795.

    https://doi.org/10.1016/j.pmatsci.2021.100795

11. Wang Z, Wang J, Xu S, *et al*., 2022, Influence of powder characteristics on microstructure and mechanical properties of inconel 718 superalloy manufactured by direct energy deposition. *Appl Surf Sci*, 583: 152545.

    https://doi.org/10.1016/j.apsusc.2022.152545

12. Hosseini E, Popovich VA, 2019, A review of mechanical properties of additively manufactured inconel 718. *Addit Manuf*, 30: 100877.

    https://doi.org/10.1016/j.addma.2019.100877

13. Cao GH, Sun TY, Wang CH, *et al*., 2018, Investigations of Γ', Γ'' and δ precipitates in heat-treated inconel 718 alloy fabricated by selective laser melting. *Mater Charact*, 136: 398–406.

    https://doi.org/10.1016/j.matchar.2018.01.006

14. Wan HY, Zhou ZJ, Li CP, *et al*., 2018, Enhancing fatigue strength of selective laser melting-fabricated inconel 718 by tailoring heat treatment route. *Adv Eng Mater* 20: 1800307.

    https://doi.org/10.1002/adem.201800307

15. Ling LS, Yin Z, Hu Z, *et al*., 2019, Effects of the Γ''-Ni(3)Nb phase on mechanical properties of inconel 718 superalloys with different heat treatments. *Materials* (*Basel, Switzerland*), 13: 151.

    https://doi.org/10.3390/ma13010151

16. Teixeira Ó, Silva FJ, Atzeni E, 2021, Residual stresses and heat treatments of inconel 718 parts manufactured via metal laser beam powder bed fusion: An overview. *Int J Adv Manuf*

Technol, 113: 3139–3162.

https://doi.org/10.1007/s00170-021-06835-8

17. Zhang B, Xiu M, Tan YT, *et al*., 2019, Pitting corrosion of SLM inconel 718 sample under surface and heat treatments. *Appl Surf Sci*, 490: 556–567.

https://doi.org/10.1016/j.apsusc.2019.06.043

18. Li L, Gong X, Ye X, *et al*., 2018, Influence of building direction on the oxidation behavior of inconel 718 alloy fabricated by additive manufacture of electron beam melting. *Materials* (*Basel*), 11: 2549.

https://doi.org/10.3390/ma11122549

19. Hedberg YS, Qian B, Shen Z, *et al*., 2014, *In vitro* biocompatibility of CoCrMo dental alloys fabricated by selective laser melting. *Dent Mater*, 30: 525–534.

https://doi.org/10.1016/j.dental.2014.02.008

20. Wang Q, Parry M, Masri BA, *et al*., 2017, Failure mechanisms in CoCrMo modular femoral stems for revision total hip arthroplasty. *J Biomedl Mater Res B Appl Biomater*, 105: 1525–1535.

https://doi.org/10.1002/jbm.b.33693

21. Mantrala KM, Das M, Balla VK, *et al*., 2014, Laser-deposited CoCrMo alloy: Microstructure, wear, and electrochemical properties. *J Mater Res*, 29: 2021–2027.

https://doi.org/10.1557/jmr.2014.163

22. Girão DC, Béreš M, Jardini AL, *et al*., 2020, An assessment of biomedical CoCrMo alloy fabricated by direct metal laser sintering technique for implant applications. *Mater Sci Eng C*, 107: 110305.

https://doi.org/10.1016/j.msec.2019.110305

23. Dijmarescu MR, Popovici TD, Tarba IC, *et al*., 2018, An experimental study on cutting forces when machining a CoCrMo alloy. *IOP Conf Mater Sci Eng*, 400: 022019.

https://doi.org/10.1088/1757-899X/400/2/022019

24. Fernandez-Zelaia P, Nguyen V, Zhang H, *et al*., 2019, The effects of material anisotropy on secondary processing of additively manufactured CoCrMo. *Addit Manuf*, 29: 100764.

https://doi.org/10.1016/j.addma.2019.06.015

25. Bettini E, Eriksson T, Boström M, *et al*., 2011, Influence of metal carbides on dissolution behavior of biomedical CoCrMo alloy: SEM, TEM and AFM studies. *Electrochim Acta*, 56: 9413–9419.

https://doi.org/10.1016/j.electacta.2011.08.028

26. Bawane KK, Srinivasan D, Banerjee D, 2018, Microstructural evolution and mechanical properties of direct metal laser-sintered (DMLS) CoCrMo after heat treatment. *Metallurgical Mater Trans A*, 49: 3793–3811.

https://doi.org/10.1007/s11661-018-4771-4

27. Cornacchia G, Cecchel S, Battini D, *et al*., 2022, Microstructural, mechanical, and tribological characterization of selective laser melted CoCrMo alloy under different heat treatment conditions and hot isostatic pressing. *Adv Eng Mater*, 24: 2100928.

https://doi.org/10.1002/adem.202100928

28. Wen Y, Zhang B, Narayan RL, *et al*., 2021, Laser powder bed fusion of compositionally graded CoCrMo-inconel 718. *Addit Manuf*, 40: 101926.

https://doi.org/10.1016/j.addma.2021.101926

29. Khanna AS, 2018, High-temperature oxidation. In: Kutz M, editor. Handbook of Environmental Degradation of Materials. 3rd ed., Ch. 6. William Andrew Publishing, Norwich, NY, p117–132.

https://doi.org/10.1016/B978-0-323-52472-8.00006-X

30. Oje AM, Ogwu AA, 2017, Chromium oxide coatings with the potential for eliminating the risk of chromium ion release in orthopaedic implants. *R Soc Open Sci*, 4: 170218.

https://doi.org/10.1098/rsos.170218

31. Tsai SC, Huntz AM, Dolin C, 1996, Growth mechanism of Cr2O3 scales: Oxygen and chromium diffusion, oxidation kinetics and effect of yttrium. *Mater Sci Eng A*, 212: 6–13.

https://doi.org/10.1016/0921-5093(96)10173-8

32. Mayrhofer PH, Rachbauer R, Holec D, *et al*., 2014, 4.14-protective transition metal nitride coatings. In: Hashmi S, Editor-in-Chief. Comprehensive Materials Processing. Elsevier, Oxford, p355–388.

https://doi.org/10.1016/B978-0-08-096532-1.00423-4